Quantitative comparison of deep-reading well resistivity to 3D CSEM at Wisting

Jan Petter Morten, EMGS, Helene Hafslund Veire and John Reidar Granli, OMV Norge, Pål T. Gabrielsen, EMGS*

Summary

We compare resistivity results from 3D CSEM and deep directional well measurements at the Wisting discovery in the Barents Sea. Measurements from the horizontal appraisal well Wisting Central II images a 2D profile of the reservoir along the well trajectory. We computed the anomalous transverse resistivity, and find that the results from surface and downhole measurements quantitatively agree. This establishes that the CSEM data captures an intrinsic reservoir property despite the lack of resolution to reservoir-scale structure, and that it is valid to do quantitative characterization using CSEM derived results. We demonstrate how the extrapolation of a stratigraphic reservoir model interpretation can be compared to CSEM inversion results to determine reservoir property variations.

Introduction

Wisting was discovered in 2013 by well 7324/8-1, which encountered an excellent quality high-resistive reservoir at burial depth only 250 m. Such a target has very high CSEM sensitivity, and a resistive CSEM anomaly had been identified before drilling from data aquired 2008. The favorable CSEM conditions boded sophisticated resistivity imaging in the Wisting area. This was recognized and inversion using a broad-band frequency spectrum led to significant imaging enhancement. A dense 3D CSEM survey with a source waveform including high frequencies up to 22 Hz was acquired in 2014. The new dataset enabled high-resolution CSEM resistivity models see Figure 1 (top). Several integration and imaging projects have studied structural and quantitative details, and this will be described in a separate manuscript (Granli et al., 2017).

To further appraise the field in the Central segment, a challenging horizontal appraisal well was recently drilled, being the shallowest and northern-most horizontal well in Norway. Field economics strongly benefit from horizontal wells, while the shallow depth introduces challenges related to well design and placement, data acquisition, and completion. Hence, the two primary objectives of the well were to assess the technical feasibility of drilling a cost-effective high dogleg horizontal well, and to test the productivity by a drillstem test (DST) in the horizontal section (Hollinger et al., 2017). The CSEM results were contributing in the well placements and to assess the fluid contact depth during well planning to ensure maximum reservoir exposure of the well. A relatively thin reservoir with high resistivity contrasts is favorable for combined well placement and reservoir mapping (structure and fluid)

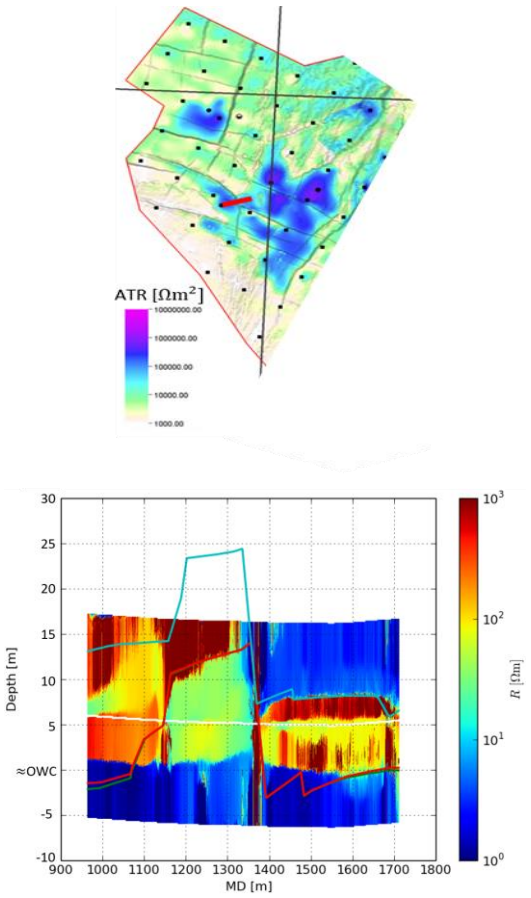

Figure 1 Top: Wisting anomalous transverse resistance from 3D CSEM. The receivers are shown as black circles and are spaced 2 km. The Wisting Central II horizontal well path is shown as a red line. Bottom: 2D mean resistivity profile along well path from the deep-reading resistivity tool. The horizontal axis shows measured depth, and the vertical axis shows vertical depth. Seismic interpreted top reservoir and top Fruholmen fm are shown as superimposed solid lines.

utilizing ultra-deep logging-while-drilling (LWD) resistivity technology. Such tool was deployed in the well for geosteering, providing a reservoir-scale image. This 2D resistivity profile is shown in Figure 1 (bottom).

We describe the calibration of 3D CSEM results to the deep-reading resistivity profile, using anomalous transverse resistance (ATR) to close the gap between the very different spatial resolutions of well and surface data. Since the two

resistivity results are obtained using measurements at very different frequency ranges (kHz and Hz), in very different environments (downhole and seafloor), and with different source and polarization, it is important to determine whether the two measurements give the same quantitative result for the reservoir resistivity. Our results confirm that reservoir characterization can be carried out by extrapolating the model interpreted from well data using the lateral coverage of 3D CSEM. A simple example of such extrapolation will be discussed.

Deep directional resistivity results in Wisting Central II

The Wisting Central II well data acquisition included deep-reading directional resistivity measurements. The tool depth penetration can exceed 30 m. In the Wisting Central II horizontal well this allows a 2D profile reservoir-scale view along the well trajectory (Figure 1 bottom). The tool makes use of long source-receiver offsets and a broad range of measurement frequencies to achieve this depth penetration as well as sensitivity in a broad range of formation resistivities, see Seydoux et al. (2014). Imaging results are achieved in real-time to optimize steering of the drillbit and provide images of the reservoir including the oil-water-contact. These results have been used to refine the geological reservoir model.

The resistivity imaging result in Figure 1 bottom represents the mean resistivity from stochastic inversion. These results are derived from a quantitative procedure, but absolute calibration of the electromagnetic field measurements depends on many details of the downhole environment. We have compared to LWD resistivity logs and find that the measured resistivity results are in quantitative agreement where the conventional resistivity tool is robust. The 1D stochastic inversion is applied to data from small segments along the well path. The ensemble of models defines the local resistivity probability distribution as a function of measured depth and distance from the wellbore, see Figure 2 top. We assume that the clean sand reservoir layers are electrically isotropic (Ellis et al., 2009). The lognormal probability distribution was estimated from resistivity quantiles of the model distributions (Figure 2, bottom) and determines a mean resistivity R with a standard deviation δR at each point. The inversion process is however biased to suppress layers in the model where the resistivity cannot be constrained by the measured data. This means that the standard deviation will be underestimated in layers with low sensitivity due to e.g. long distance from the wellbore or limited response in an unfavorable environment.

The integral of resistivity over the thickness of the reservoir is of special importance to CSEM since it is the intrinsic reservoir parameter captured by the measurement irrespective of the low vertical resolution. We can obtain this

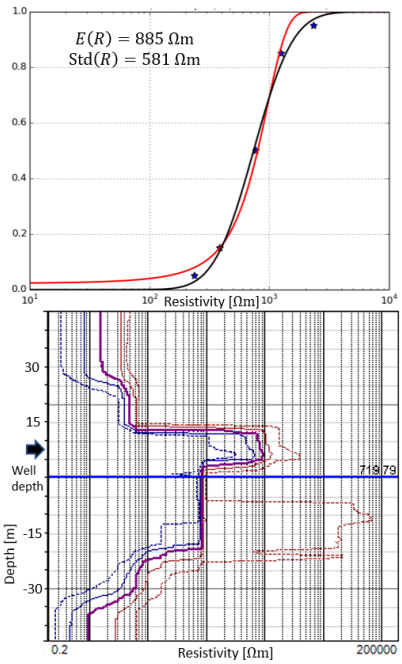

Figure 2 Top panel: Cumulative probability distribution extracted at specific measured depth and distance from the wellbore (black arrow bottom panel), black curve lognormal, red curve normal distribution. Bottom panel shows the 5, 15, 50, 85, and 95 % quantiles of the plane-layer resistivity models from stochastic inversion at this measured depth.

quantity from 2D profiles such as shown in Figure 1 as

$$\mathrm{ATR} = \sum_i \Delta z_i \left(R_i - R_i^{\mathrm{Background}}\right).$$

This defines the ATR at each lateral position along the well path as an integral over the vertical layers with index i that have thickness Δz_i. The background resistivity $R_i^{\mathrm{Background}}$ should represent the water-saturated reservoir resistivity. The standard deviations from the lognormal probability distribution defines the ATR uncertainty,

$$(\delta\mathrm{ATR})^2 = \sum_i \left(\frac{\partial \mathrm{ATR}}{\partial R_i}\delta R_i\right)^2 = \sum_i (\Delta z_i \delta R_i)^2.$$

The ATR from the deep-reading resistivity profile shown in Figure 3 will be quantitatively compared to CSEM results.

CSEM inversion and transverse resistance concept

A dense 3D CSEM survey was acquired for detailed 3D CSEM characterization of Wisting and nearby prospectivity in July 2014. We have carried out a constrained anisotropic 3D inversion of this data including frequencies up to 22 Hz. The constraints applied introduced a bias against high-resistivity zones in depth intervals above and below the reservoir. There are resistive anomalies present in the deeper

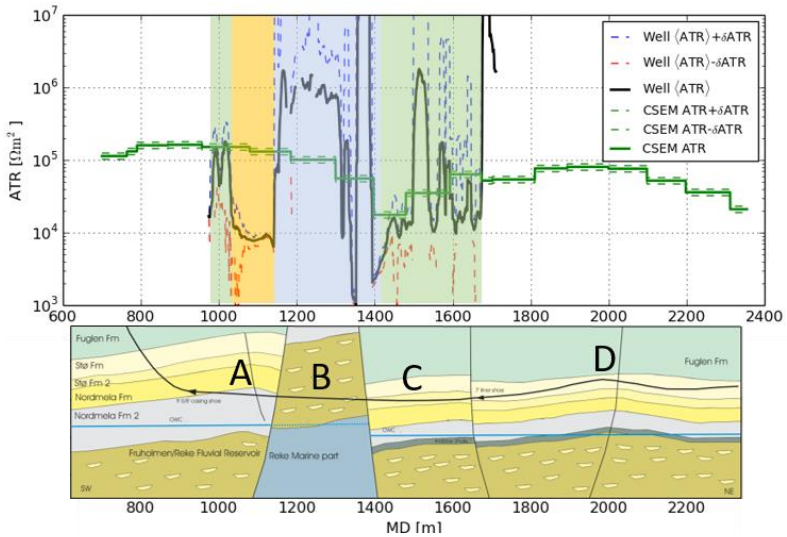

Figure 3 Top: Comparison of ATR from deep-reading resistivity measurements (black curve) and 3D CSEM inversion (green curve). The two resistivity results have a good quantitative match in the green highlighted regions. In the orange and blue highlighted regions, the discrepancies are due to sensitivity issues see main text. Bottom: Geological stratigraphy model along the well path, with a matching horizontal scale to the top panel. The letter annotation A..D identifies various sections referred in the main text. The section drilled through the Horst structure is marked B.

Triassic section as well, thus the constraint was not applied there. The reservoir thickness was defined from seismic interpretation at the Cretaceous and Jurassic levels. No constraint was applied within the reservoir depth interval in the model, thus the lateral reconstruction of reservoir resistivity is not biased in the inversion result.

The image in Figure 3 top shows the ATR recovered from both the deep-reading resistivity tool and the 3D CSEM anisotropic constrained inversion, for the reservoir at Cretaceous and Jurassic levels. We consider the CSEM vertical resistivity component, which has largest sensitivity to the reservoir resistivity variation from hydrocarbon saturation. The inversion result has a good fit to the observed data on the scale of the estimated data uncertainty. Although CSEM data do not resolve the reservoir resistivity and thickness individually, it has been shown theoretically that the ATR determines the CSEM response and represents an intrinsic reservoir parameter that can be quantified using CSEM inversion (Constable and Weiss, 2006; Mittet and Morten, 2013). This theoretical result was obtained for plane-layer models, but we have performed numerical tests that confirm that this property of the CSEM data holds with good accuracy for reservoirs with vertically-varying resistivity and 3D geometry.

As an independent test using field data, we have also compared the ATR estimate from CSEM to the resistivity logging results from exploration wells in the Wisting area to confirm the quantitative nature of the measurement. Those calibrations used data from vertically drilled wells and can only give a point calibration with more uncertainty regarding the effects of anisotropy compared to the horizontal Wisting Central II well deep-reading resistivity results discussed here.

One effect that complicates the ATR recovery from inversion is that geometrical variations related to narrow structures and edge zones diminishes CSEM sensitivity and therefore reduces our ability to reconstruct the ATR accurately. We performed forward modeling tests to estimate the resistivity uncertainty. This was done by changing the ATR systematically in the inverted model and studying the change in the fit of synthetic data to observed data. We found that in areas where CSEM sensitivity is good, the ATR is determined within a ± 10 % range in our result. Along the Wisting Central II well path, a narrow geometrical feature related to a Horst structure leads to a local ATR variation. The modeling showed that the present CSEM data have low sensitivity to this feature, and therefore the ATR is locally more uncertain at the Horst.

Calibration of ATR

The quantitative comparison of the ATR results from 3D CSEM and deep-reading resistivity profile is shown in Figure 3 top. The well results are shown with a black solid line for the mean value, and dashed lines show the range of one standard deviation. The CSEM result is shown as a dark green curve along with 10 % variation. In the green highlighted zones (first half of section A, and the section C) there is an overall quantitative fit between the CSEM and well results. Section D in Figure 3 shows the lateral variation of the CSEM result along the well trajectory in a segment where the deep-reading resistivity tool was not deployed. In the orange and blue highlighted zones, the discrepancy between the two results can be understood from sensitivity issues explained below. The agreement between the two

results provides an important calibration point for the use of CSEM-derived resistivity results in reservoir characterization. The real data results show that the ATR determined from the surface data matches the ATR obtained by downhole measurements. Therefore, it is valid to use CSEM results in quantitative reservoir characterization to extrapolate models based on well data, and we will show an example below.

For some regions in Figure 3 the well and 3D CSEM ATR results quantitatively disagree. In the orange highlighted region, the well path entered a high-resistive reservoir sand (Nordmela Fm 2 in the bottom panel). It is possible to show by modeling that the local resistivity conditions at the wellbore and the large distance to the top high-resistive reservoir sand causes the uppermost part of the section to be underestimated. This sensitivity effect is not captured in the estimated standard deviation due to a bias build into the inversion methodology. In the blue highlighted region, it is the 3D CSEM resistivity that underestimates the ATR. This is because the local reservoir geometry changes abruptly at the Horst at section B in Figure 3 bottom. The low-resolution CSEM is not sufficiently sensitive to the resistive contribution within the "peak". Since the two regions of disagreement between the ATR results are due to sensitivity issues, we do not deem these discrepancies to generally represent a problem with the quantitative joint interpretation of ATR from the well and CSEM data.

Extrapolating the reservoir characterization

In Figure 4 we co-visualize unconstrained inversion results from real data and results from a stratigraphic reservoir resistivity model based on the geological model shown in Figure 3. As part of the interpretation methodology described in Granli et al. (2017), the real and synthetic data sets were imaged using the same data coverage and inversion settings. The average vertical resistivity in the two inversion results was extracted from a depth interval at the target level, and is shown as curves in the figure using the well path as the ordinate. The reservoir resistivities in the model stratigraphic units were uniform, but the model accurately represents the reservoir-scale geometry of the layers. We see that left of the Horst, the agreement between the two models is very good (black and red curves overlap). The stratigraphic reservoir resistivity model was based on the deep-reading resistivity data from this interval, and the agreement is then expected at this calibration point. On the right side of the Horst, we see that the real data result indicates lower resistivity than the model (highlighted by grey ellipse). Such variation can be understood as a change in reservoir quality, since also the well data indicated some change in properties. Another region of discrepancy between the results is highlighted by the lower right grey ellipse. This region is approaching a fault zone where the resistivity

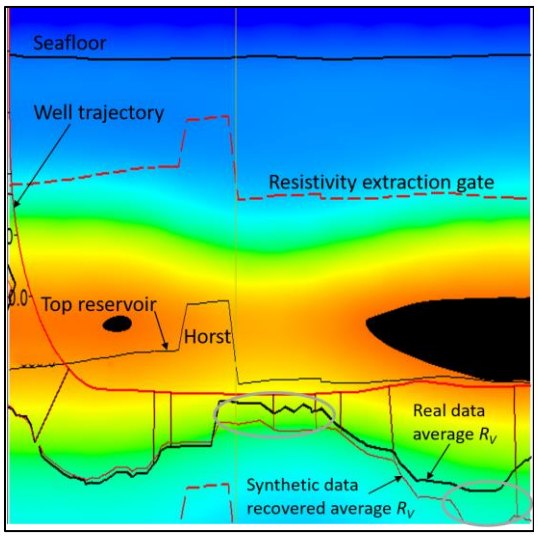

Figure 4 Comparison of unconstrained inversion results from 3D stratigraphic reservoir resistivity model and real data. The unconstrained synthetic data inversion result is shown as color-coded background. The average resistivity from the real data and that recovered from the model is graphed using the well trajectory as the ordinate.

properties may be locally affected causing the homogeneous-layer model to overestimate resistivity.

Conclusion

At the inception of 3D CSEM for hydrocarbon exploration more than fifteen years ago, the value of the technology for drill-or-drop decisions was clear from anomaly identifications in field tests. Substantial improvements have made it possible to apply the technology also for detailed field delineation and resource estimation. The next step is to extract quantitative reservoir property information, but this is not straightforward due to the lack of resolution to reservoir-scale structure. Theoretical work has established that the reservoir ATR is quantitatively captured by the data. The work presented in this abstract validates the quantitative nature of CSEM derived ATR using field data and downhole measurements. The outlook now is to use the CSEM view into an intrinsic reservoir parameter to characterize reservoir stratigraphy, facies, fault-zone properties and extract further value in field development.

Acknowledgements

We thank OMV Norge and EMGS for permission to publish these results. We also thank the PL537 partners Statoil, Idemitsu, and Petoro for support. We acknowledge technical discussions and support from C. Dupuis and H. Wang at Schlumberger for the deep directional resistivity measurements, and colleagues K. Birkeland, E. Stueland, and B. Sigvathsen for important contributions.

EDITED REFERENCES

Note: This reference list is a copyedited version of the reference list submitted by the author. Reference lists for the 2017 SEG Technical Program Expanded Abstracts have been copyedited so that references provided with the online metadata for each paper will achieve a high degree of linking to cited sources that appear on the Web.

REFERENCES

Ellis, M., M. Sinha, and R. Parr, 2010, Role of fine-scale layering and grain alignment in the electrical anisotropy of marine sediments: First Break, **28**, 49–57, https://doi.org/10.3997/1365-2397.2010021.

Granli, J. R., H. Hafslund Veire, P. T. Gabrielsen, and J. P. Morten, 2017. Maturing broadband 3D CSEM for improved reservoir property predictions in the Realgrunnen Group at Wisting, Barents Sea: 87th Annual International Meeting, SEG, Expanded Abstracts, Submitted 2017.

Hollinger, G., S. Trauner, C. Dupuis, A. S. Wendt, D. H. Breivik, and O. H. Myrvoll, 2017, Transformation of mindset — Cost-effective collaborative well engineering & operation delivers record horizontal appraisal well in the barents: SPE/IADC Drilling Conference and Exhibition, SPE-184654-MS, https://doi.org/10.2118/184654-MS.

Mittet, R., and J. P. Morten, 2013, The marine controlled-source electromagnetic method in shallow water: Geophysics, **78**, no. 2, E67–E77, https://doi.org/10.1190/geo2012-0112.1.

Seydoux, J., E. Legendre, E. Mirto, C. Dupuis, J.-M. Denichou, N. Bennett, G. Kutiev, M. Kuchenbecker, C. Morriss, and L. Yang, 2014, Full 3d deep directional resistivity measurements optimize well placement and provide reservoir-scale imaging while drilling: 55th Annual Logging Symposium, SPWLA.

Weiss, C. J., and S. Constable, 2006, Mapping thin resistors and hydrocarbons with marine EM methods: Part 2 — Modeling and analysis in 3D: Geophysics, **71**, no. 6, G321–G332, https://doi.org/10.1190/1.2356908.